Utilizing BP neural networks to accurately reconstruct the tritium depth profile in materials for BIXS[*]

Chen Zhao,[1] Wei Jin,[1] Yan Shi,[1] Chang-An Chen,[1, †] and Yi-Ying Zhao[1, ‡]

[1]*Institute of Materials, China Academy of Engineering Physics, Jiangyou 621908, China*

β-ray-induced X-ray spectroscopy (BIXS) is a promising method for tritium detection in solid materials because of its unique advantages, such as large detection depth, nondestructive testing capabilities, and low requirements for sample preparation. However, high-accuracy reconstruction of the tritium depth profile remains a significant challenge for this technique. In this study, a novel reconstruction method based on a backpropagation (BP) neural network algorithm that demonstrates high accuracy, broad applicability, and robust noise resistance is proposed. The average reconstruction error calculated using the BP network (8.0%) was much lower than that obtained using traditional numerical methods (26.5%). In addition, the BP method can accurately reconstruct BIX spectra of samples with an unknown range of tritium and exhibits wide applicability to spectra with various tritium distributions. Furthermore, the BP network demonstrates superior accuracy and stability compared to numerical methods when reconstructing the spectra, with a relative uncertainty ranging from 0 to 10%. This study highlights the advantages of BP networks in accurately reconstructing the tritium depth profile from BIXS and promotes their further application in tritium detection.

Keywords: β-ray-induced X-ray spectroscopy, Tritium detection, BP network, Ridge regression, Reconstruction problem

I. INTRODUCTION

The development of a nondestructive detection technique for measuring tritium content and distributions in solid materials is essential for understanding the tritium permeation process in fields such as fusion research [1–8]. Among such methods, β-ray-induced X-ray spectroscopy (BIXS) has distinct advantages, including a large detection depth, low sample requirements, and convenient testing [9–16]. The β-rays emitted from tritium excite X-ray emission from the base materials and testing gas. The resulting X-ray spectrum contains information on the tritium depth profile in the materials. However, reconstruction of the tritium depth profile using BIXS is a significant challenge because of its underdetermined, nonlinear, and ill-posed nature and needs to be urgently addressed for further application of BIXS [17].

Numerous studies have reconstructed tritium depth profiles from BIXS using classical numerical methods. Matsuyama et al. used a semi-empirical formula to calculate theoretical BIX spectra based on various assumed tritium distributions. The tritium depth profiles were then inferred by comparing the calculated and measured BIX spectra [18]. However, this reconstruction method has difficulty in handling BIX spectra with complex tritium distributions and fails to address the ill-posed nature of the inverse problem. An et al. utilized Monte Carlo methodology to simulate the BIX spectra and introduced the Tikhonov regularization method, also known as ridge regression, to reconstruct the tritium depth profile [19]. The reconstruction error ranged from 2% to 40% with varying relative uncertainties and regularization codes. The accuracy of the reconstruction results depended on the accuracy of testing. Furthermore, BIXS data obtained from a sample with an unknown tritium distribution depth cannot be resolved using this method. Therefore, it is necessary to develop a reconstruction method with higher accuracy and broader applicability to improve the tritium detection capability of BIXS.

Classical numerical methods for BIXS reconstruction, such as ridge regression, inevitably face ill-posed equations. In contrast, an artificial neural network (ANN) algorithm may bypass this difficulty and directly model the complex and nonlinear relationships between the tritium depth profile and X-ray spectrum [20–23]. This capability can significantly improve the reliability and accuracy of reconstruction [24–26]. Numerous studies have highlighted the advantages of ANN algorithms in addressing inverse and unfolding problems in radiation detection [27–33]. Bagherzadeh-Atashchi et al. developed an ANN model to unfold the neutron energy spectrum and achieved a final error of less than 10% [34]. Jorge et al. utilized a multilayer perceptron (MLP) neural network to reconstruct linear accelerator spectra and achieved a high concordance between 92% and 96% [35]. Given the analogous nature of various radiation detection reconstruction challenges, employing the ANN algorithm holds promise for achieving high-accuracy reconstruction of BIXS.

In this study, we propose a high-accuracy reconstruction approach for BIXS based on an ANN algorithm. Owing to their wide-ranging applicability, a backpropagation (BP) neural network was constructed and trained to reconstruct tritium depth profiles from BIX spectra. A Monte Carlo model was developed to simulate the BIX spectra as a training database for the BP network. The number of neurons in the hidden layer of the network was optimized to minimize reconstruction errors. The reconstruction accuracies of the tritium depth profiles obtained from the BP network and traditional ridge regression were then compared using different distribution profiles. The BP network reconstruction algorithm had a lower average error of 8.0% compared to ridge regression, which had an average error of 26.5%. This was attributed to the high applicability of the BP network to different types of
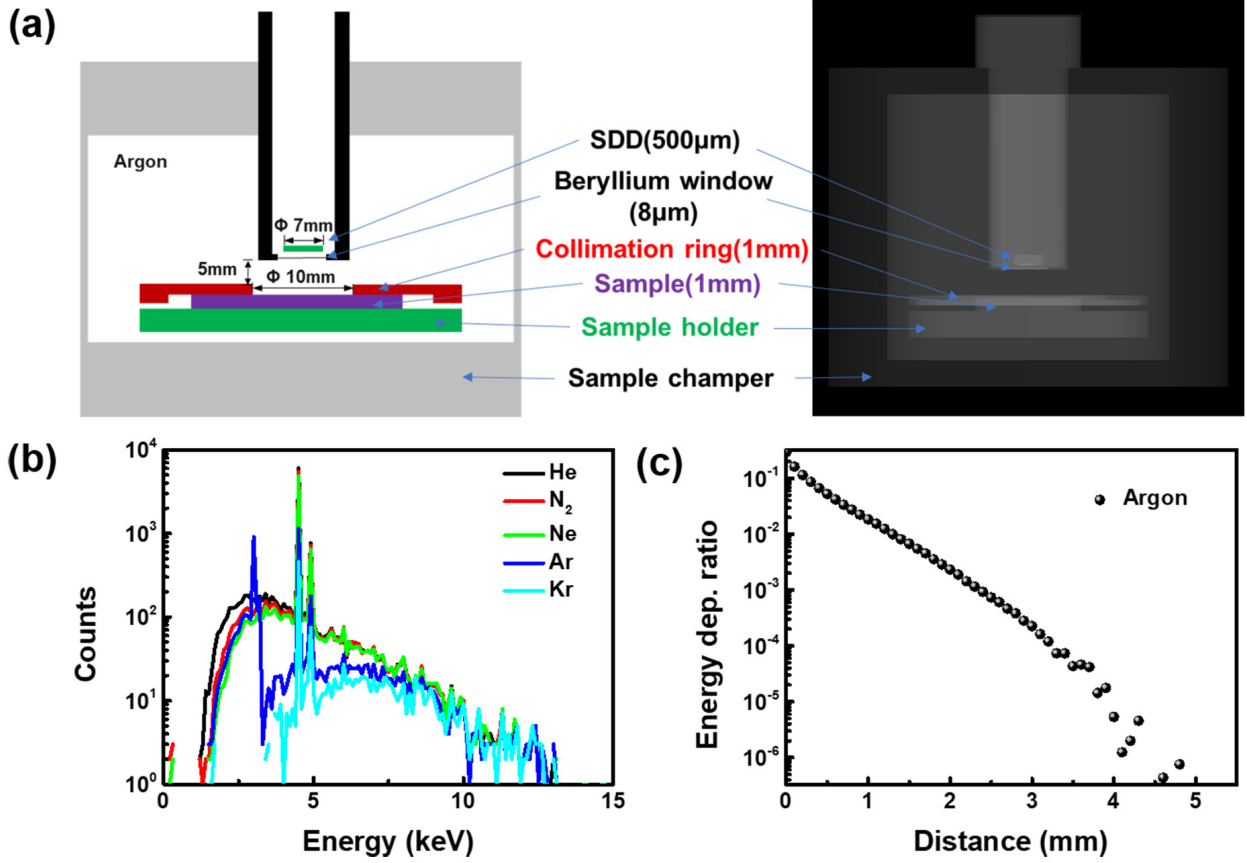

Fig. 1. (Color online) (a) Schematic of a BIXS device based on a silicon drift detector (SDD) (left) and a model built in the Monte Carlo simulation code Geant4 (right). (b) Calculated BIX spectra of a tritiated titanium sample in various atmospheres, including helium, nitrogen, neon, argon, and krypton; each spectrum was simulated using Geant4 with 10^8 electrons. (c) Energy deposition profile of β particles emitted from tritium in argon.

distributions and its ability to solve the BIX spectra of samples with an unknown range of tritium. The results of this study demonstrate the great potential of the ANN algorithm as a high-accuracy reconstruction method for BIXS.

II. METHODS

A. Monte Carlo simulations of BIXS

The training of an ANN requires large amounts of BIXS data, including the X-ray spectra and corresponding tritium depth profiles. However, this is difficult owing to the control of tritiated samples. Therefore, a Monte Carlo model was built using Geant4 code to simulate the BIX spectra, which has been proven to be highly accurate in previous studies [4, 9, 36]. The left side of Fig. 1(a) shows a schematic of a BIXS device based on a silicon drift detector (SDD), which are known for their high sensitivity to soft X-rays. This type of detector is commonly employed in BIXS studies [12, 36]. The geometry of the SDD used in our model was based on an AXAS-D-H30 SDD manufactured by KETEK. The SDD had a diameter of 7 mm and thickness of $500\,\mu$m. The beryl-

lium window on the SDD had a thickness of $8\,\mu$m. A tritiated sample was placed on a sample holder, and a collimation ring with an inner diameter of $10\,$mm was used to standardize the X-ray emission area. The entire system was placed in a sample chamber.

The corresponding model built in Geant4 is shown on the right-hand side of Fig. 1(a), encompassing all the primary components of a practical BIXS device to enhance the precision of the simulation. Tritium atoms were set in the sample region and generated using the G4GeneralParticleSource module. The tritium decay process was simulated using the G4RadioactiveDecayPhysics module, and the electron energy spectrum was set to the default Geant4 value. The energy range of β particles emitted from the tritium was 0–18.6 keV, with an average energy of $5.7\,$keV. The β particles were emitted isotropically in all directions within a 4π solid angle. The electromagnetic interactions between the electrons and materials were simulated using the PENELOPE model implemented in Geant4. Fluorescent X-rays and Auger transitions were considered in the simulations to enhance the accuracy of the calculated BIX spectra. The SDD shape was designated as the sensitive volume, and the BIX spectra were obtained by analyzing the energy distribution of the X-rays penetrating
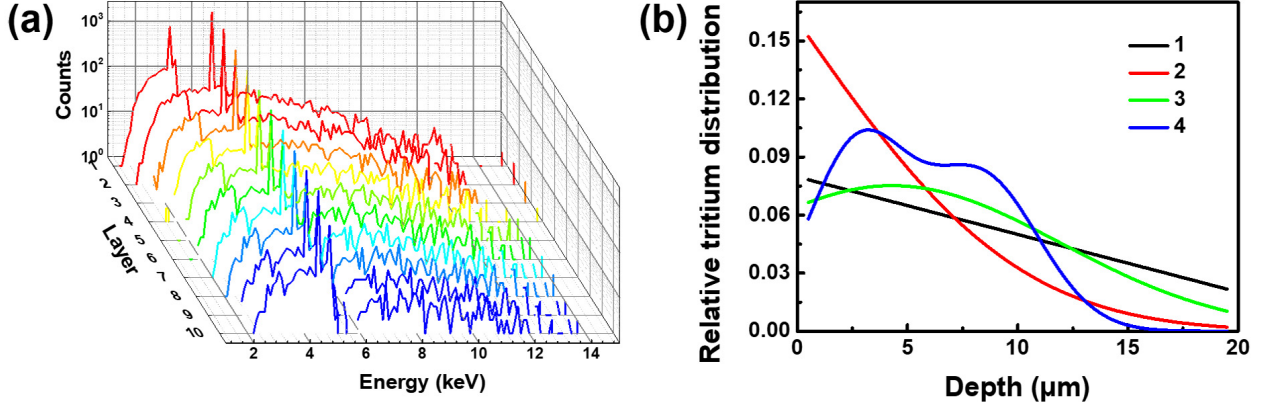
Fig. 2. (Color online) (a) Calculated BIX spectra of a titanium sample with tritium distributed at different depths in semi-logarithmic coordinates; layer i represents tritium evenly distributed in a depth range of $(i-1)$ μm to i μm. (b) Four tritium depth profiles that describe the (1) steady-state diffusion, (2) unsteady-state diffusion, (3) single-energy implantation, and (4) dual-energy implantation of tritium.

the SDD using the G4AnalysisManager module. The cutoff energy of the particles simulated in Geant4 was set at $100\,\mathrm{eV}$, and the cutoff length was set at $10\,\mathrm{nm}$ to ensure a high simulation accuracy.

The atmosphere in the BIXS system and the distance between the surface of the SDD and the sample were optimized using a model built in Geant4. Fig. 1(b) shows the calculated BIX spectra of a tritiated titanium sample under various atmospheres, including helium, nitrogen, neon, argon, and krypton gases. Each spectrum was simulated using 10^8 electrons in Geant4 and divided into 186 bins ranging from $0\,\mathrm{keV}$ to $18.6\,\mathrm{keV}$. Most β particles emitted by the tritium stopped in the titanium sample, resulting in the generation of characteristic X-rays and bremsstrahlung. Therefore, all the X-ray spectra show two characteristic peaks, at $4.5\,\mathrm{keV}$ and $4.9\,\mathrm{keV}$, corresponding to the K_α and K_β lines of titanium. The β-rays emitted from the tritium at a superficial depth exit the sample and excite the X-rays of the atmospheric gas. The BIX spectra obtained from atmospheres of helium, nitrogen, and neon exhibited only two characteristic titanium peaks. This is because the characteristic X-ray energies of these gases are considerably low, typically below $1\,\mathrm{keV}$. Consequently, the beryllium window absorbs the characteristic X-rays and causes the lack of corresponding peaks. The characteristic X-ray energy of krypton is very high, at $12.6\,\mathrm{keV}$. However, the efficiency of exciting krypton gas is hindered by the low energy of the β particles emitted by the tritium. The characteristic X-ray energy of argon is moderate, at $2.96\,\mathrm{keV}$, leading to a distinct peak in the BIX spectrum, as shown in Fig. 1(b). The intensity of the characteristic peak of the atmospheric gas reflects information on the tritium in the shallow regions of the sample, which is essential for reconstruction. Therefore, argon was selected as the testing environment, which is consistent with most previous studies [14, 36, 37]. Fig. 1(c) shows the energy deposition ratio of β particles emitted by tritium in argon at 1 atm. The energy of the β particles deposited in the argon gas decays

exponentially, and a $5\,\mathrm{mm}$-thick layer of argon gas can fully absorb the energy. Therefore, the distance between the surface of the SDD and the sample was set to $5\,\mathrm{mm}$ to convert all the β particle energy into characteristic X-rays. The Monte Carlo simulation described in the following section used the same settings.

B. Construction of training dataset

Fig. 2(a) shows the calculated BIX spectra of a tritiated titanium sample as a function of tritium depth. The parameters of the BIXS device were the same as those described above. The BIX spectra of Layers 1–20 were calculated when the tritium was evenly distributed in each layer. The ith layer represents the distribution of tritium within the range from $(i-1)$ μm to i μm. Only the first ten layers are shown in Fig. 2(a). The total number and thickness of the layers could be adjusted based on the specific requirements of the BIXS test. All the X-ray spectra show two characteristic peaks, at $4.5\,\mathrm{keV}$ and $4.9\,\mathrm{keV}$, corresponding to the K_α and K_β lines of titanium, as shown in Fig. 1(b). In addition, the total count of the X-ray spectra decreases as the depth of the layer increases. A portion of the X-rays generated inside the titanium was self-absorbed by the sample. A greater tritium depth results in a reduced proportion of detected X-rays. X-rays with lower energies exhibited a greater degree of self-absorption, leading to a rapid change of BIX spectrum shape on the low-energy side. The BIX spectrum of Layer 1 shows an additional characteristic peak at $3.0\,\mathrm{keV}$, corresponding to the K_α line of argon. As mentioned above, the β-rays emitted from the tritium in shallower layers exit the sample and excite the X-rays from the argon, whereas those emitted in a deeper layer are absorbed by the sample, resulting in the absence of the characteristic argon peak.

The final BIX spectrum contains information on tritium at different depths with different weights. Therefore, it can be

obtained using the following equation:

$$S(E) = \sum_{i=1}^{20} f(i)S_i(E), \qquad (1)$$

where $S(E)$ is the final X-ray spectrum obtained from the BIXS device; f(i) is the relative tritium content at the ith layer, that is, the value of the probability distribution function $f(x)$ when $x = i$; and $S_i(E)$ is the BIX spectrum with tritium distributed at the ith layer, as shown in Fig. 2(a). Four different tritium distribution functions were used to replicate the practical depth profiles of tritium in the samples, as shown in Fig. 2(b). The first two functions describe the distribution caused by tritium diffusion and the last two describe tritium implantation [38–41]. These four functions describe the steady-state diffusion, unsteady-state diffusion, single-energy implantation, and dual-energy implantation of tritium. The specific probability distribution function for each type of distribution is described by Equations 2–5:

$$f_1(x) = kx + b, \qquad (2)$$

$$f_2(x) = k[1 - erf(bx)] + c, \qquad (3)$$

$$f_3(x) = \frac{1}{\sqrt{2\pi}\sigma} exp(-\frac{(x-u)^2}{2\sigma^2}) + c, \qquad (4)$$

$$f_4(x) = \frac{k_1}{\sqrt{2\pi}\sigma_1} exp(-\frac{(x-u_1)^2}{2\sigma_1^2}) + \\ \frac{k_2}{\sqrt{2\pi}\sigma_2} exp(-\frac{(x-u_2)^2}{2\sigma_2^2}) + c, \qquad (5)$$

where k, b, σ, u, and c are the coefficients of the functions that determine the detailed depth profiles, and erf is the Gaussian error function. These four distributions were selected with equal probability to generate the corresponding final BIX spectrum using Eq. (1). In addition, the coefficients in each distribution were randomly selected within a reasonable range to ensure that each BIX spectrum corresponded to a depth profile of a unique shape. The detailed range of each coefficient is provided in Table 1. The final randomly generated probability distribution function was normalized to ensure that the total probability equaled one. The generated database was used to train the BP network and test the reconstruction accuracy of both the network and the ridge regression.

C. Structure of the BP network

Fig. 3 shows the structure of the BP network used in this study for BIXS reconstruction. It consisted of three layers: input, hidden, and output. The input layer consisted of 186 neurons, each corresponding to one of the 186 bins in the BIX spectrum. The output layer consisted of 20 neurons that
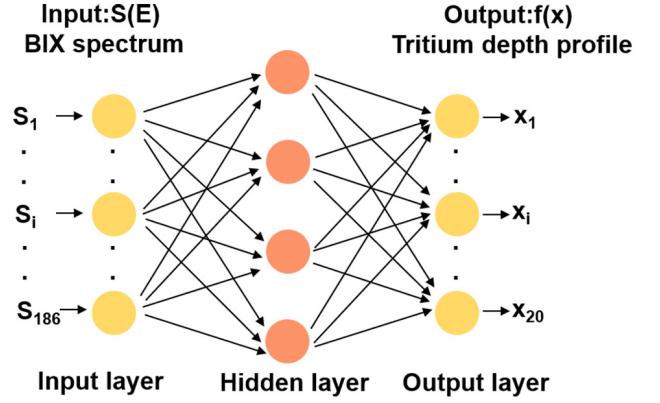

Fig. 3. (Color online) Structure of the backpropagation network used for reconstructing the tritium depth profiles from BIX spectra

represented the values of the probability distribution function within the range 0–20 μm. The three layers in the network were fully connected, meaning that each neuron in the previous layer was connected to all neurons in the next layer. In addition, the network was trained using an error backpropagation algorithm. The training process of a BP network optimizes the connection coefficients to minimize error, which helps the network accurately establish nonlinear relationships between the tritium depth profiles and BIX spectra. The BP network was written in Python 3 using the PyTorch library. A sigmoid function was used as the activation function. The activation function introduced nonlinearity into the BP network, enabling it to effectively model a wide range of curves. Sigmoid functions are commonly used nonlinear functions that transform input values into a range between zero and one. This property makes them well suited for models in which the outputs are intended to represent probabilities. The network in this study was required to output the tritium depth profile, which reflects the probabilities of the relative tritium contents at different depths. Therefore, a sigmoid function was used as the activation function. The mean square error (MSE) was used as the loss function to calculate the average of the squares of errors between the predicted values and actual labels. MSE is commonly employed as a loss function in regression problems, where it is essential to model and analyze the relationships between variables. The tritium depth profile was reconstructed based on the relative intensity of each bin in the BIX spectrum. Therefore, MSE was utilized to enhance the performance of the BP network. In addition, the reconstruction of the tritium depth profile from BIXS requires the consideration of data along with their corresponding relative uncertainties. Therefore, the adaptive moment estimation algorithm (Adam) was used as the optimization algorithm and was chosen for its suitability in handling datasets with significant volume and noise.

TABLE 1. Ranges of the coefficients used in the four distribution functions

Function 1		Function 2		Function 3		Function 4	
Coefficient	Range	Coefficient	Range	Coefficient	Range	Coefficient	Range
k	$(-0.08, 0)$	k	$(0, 1)$	σ	$(1, 10)$	k_1	$(0.4, 0.6)$
b	$(0.05, 0.4)$	b	$(0.05, 0.7)$	u	$(1, 5)$	σ_1	$(1, 5)$
		c	$(0, 0.01)$	c	$(0, 0.01)$	u_1	$(1, 5)$
						k_2	$(0.4, 0.6)$
						σ_2	$(1, 5)$
						u_2	$(6, 15)$
						c	$(0, 0.01)$

Fig. 4. (Color online) (a) Mean square errors (MSE) of the backpropagation network with 5000 hidden neurons in the training and test datasets as a function of epoch. (b) Average reconstruction errors of the backpropagation network in the training and test datasets as a function of hidden neuron number.

III.   RESULTS AND DISCUSSIONS

A.   Training of the BP network

Fig. 4(a) shows the trend of the training and testing MSE obtained by the BP network with 5000 hidden neurons as the training epochs progressed. Ten thousand pairs of different probability distribution functions and BIXS spectra were generated to train the BP network, with the training and testing datasets set at a 7:3 ratio. The BP network was trained using a single GPU with an FP32 performance of 30 TFLOPS for 10 h. The results illustrate a rapid initial decrease in the MSE, followed by leveling off in both the training and testing datasets. The MSE obtained using the BP network barely decreased after 200 epochs. The great astringency of the BP network demonstrates its effectiveness in learning the BIXS data and establishing a correlation between the BIX spectra and tritium depth profiles. Moreover, the MSE obtained for both datasets exhibit minimal divergence as the number of epochs increases, indicating no overfitting during the training process. The performance of the trained BP network was subsequently evaluated based on the average error in reconstructing the tritium depth profile (δ) as defined by the following equation presented by Long and An [19]:

$$\delta = \frac{\sum_{i=1}^{M} |a_{rec,i} - a_{ori,i}|}{\sum_{i=1}^{M} a_{ori,i}} \times 100 \qquad (6)$$

where $a_{rec,i}$ and $a_{ori,i}$ are the reconstructed and original probability distribution values at the ith layer, respectively. The value of δ obtained by BP network with 5000 hidden neurons was 11.4%. This can be further improved by increasing the number of hidden neurons, which is the primary parameter affecting the fitting capability of the BP network. Fig. 4(b) shows the average reconstruction errors of the trained BP network in the training and test datasets plotted against the number of hidden neurons. As the number of hidden neurons increases from 5000 to 40000, the value of δ decreased from 11.4% to 8.0% at a decreasing rate of change. This result shows the effectiveness of increasing the number of hidden neurons in the BP network at reducing reconstruction errors. In addition, a substantial increase in the number of hidden neurons does not lead to a significant reduction in the reconstruction error according to Fig. 4(b). The values of δ obtained in the training and test datasets were very close for each BP network, which implies that there was no overfitting with the addition of hidden neurons, indicating the outstanding quality of the BP network. Consequently, a BP network with 40000 hidden neurons was used for the subsequent reconstruction test and was compared to traditional numerical
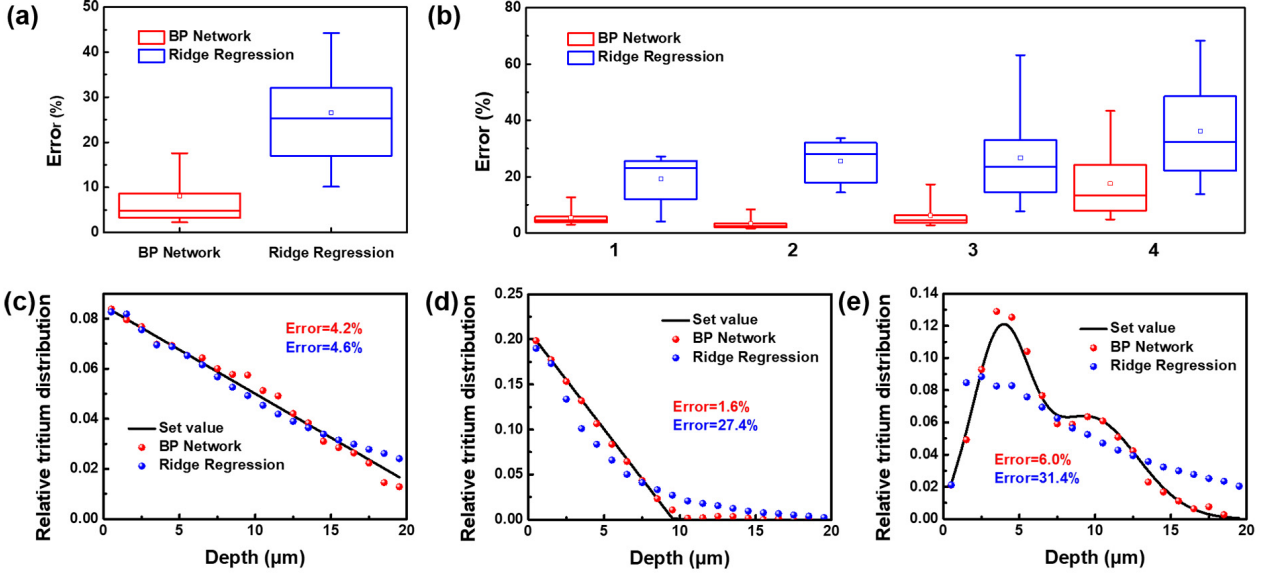
Fig. 5. (Color online) (a) Box charts for the reconstruction errors calculated by the backpropagation (BP) network and ridge regression. (b) Box charts for the reconstruction errors of BIX spectra with four distribution functions calculated by the BP network and ridge regression. True depth profile of tritium (black curve) compared to the calculated values obtained by the BP network (red scatter plots) and ridge regression (blue scatter plots) reconstructed from the BIX spectrum with (c) a 20-μm-depth steady-state diffusion distribution, (d) an unknown-depth steady-state diffusion distribution, and (e) a dual-energy implantation distribution.

methods.

B. Comparison of reconstruction accuracy

Fig. 5(a) shows box charts for the reconstruction errors calculated using the BP network and ridge regression. The charts present the mean value, median value, and 25%–75% and 5%–95% ranges of the 3000 errors calculated using the testing dataset. The ridge regression method was implemented using the RidgeCV model from the SciPy library. Ridge regression is an improved least-squares method. The tritium depth profile was calculated using the following equation:

$$x = (S_{20}^T S_{20} + \alpha I_{20}^T)^{-1} S_{20}^T S(E), \qquad (7)$$

where x is the tritium depth distribution vector, S_{20} is a matrix that contains the BIX spectra from Layers 1 to 20, α is the ridge coefficient, and I_{20} is a unit matrix. The optimal ridge coefficient for each BIX spectrum was automatically selected using a cross-validation method in the RidgeCV model. The average error of the tritium depth profiles reconstructed by the BP network was 8.0%, which was significantly smaller than that calculated by ridge regression (26.5%). In addition, the standard deviation of δ calculated by the BP network was smaller than that of the ridge regression, indicating greater reconstruction reliability.

Fig. 5(b) illustrates the detailed reconstruction errors of BIX spectra using four different distribution functions calculated using the two methods. The BP network outperformed ridge regression across all distributions. The average reconstruction errors of BIX spectra with steady-state diffusion, unsteady-state diffusion, single-energy implantation, and dual-energy implantation distributions calculated using the BP network were 5.5%, 3.5%, 6.3%, and 17.6%, respectively. The corresponding errors calculated using ridge regression were 19.2%, 25.5%, 26.7%, and 36.1%. The dual-energy implantation distribution was the most difficult to reconstruct because both methods had the largest errors when solving this distribution.

One reason for the smaller reconstruction error in the BP network is its ability to address the BIX spectrum of samples with an unknown range of tritium. Fig. 5(c) and 5(d) show the reconstruction results obtained using the two methods in comparison with the original set values. Both distributions were steady-state distributions. The sample shown in Fig. 5(c) had a 20-μm tritium distribution range, which means that all values of the probability distribution function were positive. The reconstruction error of this sample, calculated using ridge regression (4.6%), was very close to that calculated using the BP network (4.2%). The ridge regression method demonstrated the ability to effectively solve the BIX spectra of the samples with a known tritium depth range. However, the samples shown in Fig. 5(d) had an unknown distribution range, implying that some probability values were zero. The reconstruction error of this sample, calculated by ridge regression (27.4%), was much larger than that of the BP network (1.6%). Therefore, the average reconstruction error and standard deviation obtained using ridge regression were much higher than those obtained using the BP network, as shown in Fig. 5(b). The presence of zeros in the probability distribution functions
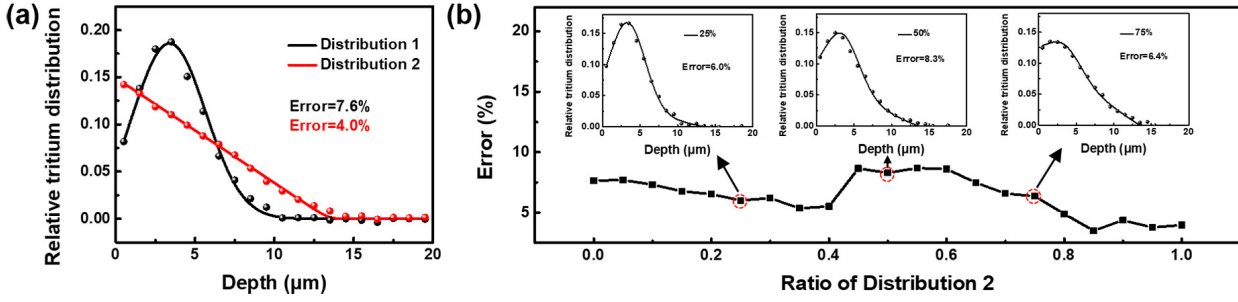
Fig. 6. (Color online) (a) True tritium depth profile (solid line) with two different distribution functions compared to the calculated values obtained by the BP network (scatter plots), marked with the reconstruction errors. (b) Reconstruction error from mixed BIX spectra as a function of the ratio of Distribution 2 using the BP network; inset: the true and reconstructed tritium depth profiles from the BIX spectrum with 25%, 50%, and 75% Distribution 2 ratios.

complicates the resolution of an ill-posed system of equations using ridge regression. Simultaneously, the strategy of randomly selecting the coefficients of the distribution function generated a substantial training dataset for the BP network. This aids the network in capturing the nonlinear relationships between the X-ray spectra and tritium depth profiles with various ranges.

Another advantage of the BP network in BIXS reconstruction is its broad applicability to various types of tritium distributions, particularly its ability to address complex tritium depth profiles. The dual-energy implantation distribution was the most complicated distribution used in this study, and the average reconstruction errors of this distribution using the BP network and bridge regression were the highest among all four distributions, as shown in Fig. 5(b). Fig. 5(e) shows a reconstruction example with the dual-energy implantation distribution obtained from the BP network and ridge regression, compared to the set value. The reconstruction error of this sample, calculated by the BP network (6.0%), was remarkably lower than that of ridge regression (31.4%), indicating the ability of the BP network to reconstruct BIX spectra with complex tritium depth profiles.

The broad applicability of the BP network was also reflected in its ability to accurately reconstruct mixed BIX spectra, indicating that there were at least two types of tritium depth profiles in the sample. Fig. 6 shows an example of the reconstruction results of BIX spectra mixed with two different types of tritium distribution functions using a BP network. Fig. 6(a) shows the two original tritium depth profiles, one of which belongs to the single-energy implantation distribution (Distribution 1), and the other to the steady-state distribution (Distribution 2). The reconstruction errors of these two distributions using the BP network were 7.6% and 4.0%, respectively. A mixed BIX spectrum was generated by combining these two tritium distribution functions in different ratios, as described by the following equation:

$$f_m(x) = \sum_{k=1}^{n} a_k f_k(x), \qquad (8)$$

where $f_m(x)$ is the mixed tritium depth profile, $f_k(x)$ is the kth-independent tritium depth profile, a_k is the ratio of kth tritium depth profile, and n is the total number of tritium depth profiles, where $n = 2$. The mixed tritium depth profile was further normalized and the mixed BIX spectrum was calculated using Eq. (1). Fig. 6(b) shows the reconstruction errors obtained from the mixed BIX spectra using the BP network plotted against the ratio of Distribution 2. The reconstruction error consistently remained below 10% across a ratio range of 0–100%, highlighting the high reconstruction accuracy of the BP network on the mixed BIX spectra. A peak reconstruction error was observed around the 50% ratio position, where the mixed BIX spectrum exhibited the most significant deviation from the two original BIX spectra. The insets in Fig. 6(b) shows the mixed tritium depth profiles with 25%, 50%, and 75% ratios of Distribution 2 along with the corresponding reconstruction results and detailed reconstruction errors. As the ratio of Distribution 2 increased, the peak of the mixed tritium depth profile became indistinct, and the tail of the curve became linear. When the ratios of the two distribution functions were equal, the mixed tritium depth profile exhibited the characteristics of both functions. The reconstructed tritium depth profiles (scatter plots) were very close to the true values, with reconstruction errors of 6.0%, 8.3%, and 6.4% at the specified ratios when using the BP network. Despite the absence of information regarding these mixed spectra in the training dataset, the BP network demonstrated a high accuracy in reconstructing these spectra. This result convincingly demonstrates the broad capability of the BP network to reconstruct BIX spectra with various tritium depth distributions.

C. Comparison of noise resistance

Noise resistance is another crucial figure of merit for the reconstruction method that reflects the accuracy and stability of the reconstruction results when the BIX spectra have additional relative uncertainties. Gaussian noise of varying intensity was added to the dataset to emulate uncertainty in the measurements. A dataset containing BIX spectra with 0–
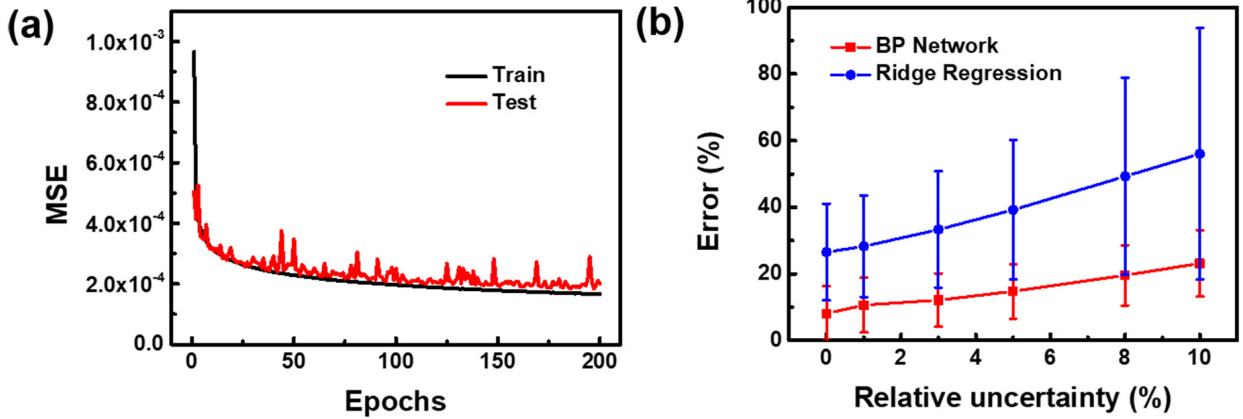
Fig. 7. (Color online) (a) Mean square errors (MSE) of the backpropagation network in the training and test datasets with 0–10% gaussian noise as a function of epoch. (b) Average error and standard deviation of errors calculated by the backpropagation network and ridge regression as a function of the relative uncertainty of the BIX spectra.

10% relative uncertainty was used to train the BP network. Fig. 7(a) shows the trend of the training and testing MSE obtained by the BP network with 40000 hidden neurons as a function of epoch. The trend in MSE obtained with a dataset containing 0–10% Gaussian noise closely resembles the pattern depicted in Fig. 4(a). The MSE of the BP network continued to exhibit significant astringency with increasing epoch, which demonstrates the effectiveness of the BP network in modeling the correlation between the tritium depth profiles and BIX spectra among varying levels of noise interference. The addition of relative uncertainties increased the variability of convergence, thereby inducing fluctuations in the MSE curve of the testing dataset. In addition, the consistency of MSE in the training and testing datasets did not exhibit the same level of perfection as shown in Fig. 4(a). However, the specific disparity was less than 10%, which indicates an ideal fit of the BP network to the dataset with a 0–10% relative uncertainty.

Fig. 7(b) presents the reconstruction errors of the tritium depth profile calculated using the BP network and ridge regression as functions of the relative uncertainty of the BIX spectra. Each point was obtained by calculating the average and standard deviation of 10000 reconstruction errors. When the relative noise of the BIX spectra increased from 0% to 10%, the average reconstruction errors calculated by the BP network increased from 8.0% to 23.2%, which is a much lower range than that of the ridge regression, which increased from 26.5% to 56.0%. In addition, the standard deviation of the errors calculated by the BP network barely increased with increasing noise, whereas those of ridge regression significantly increased from 14.5% to 37.7%. The detailed averages and standard deviations of the errors obtained using the two methods are listed in Table 2. This result demonstrates the high noise resistance of the BP network method, which is extremely important for practical BIXS applications.

Fig. 8 shows a detailed example of how additional noise in the BIX spectrum affects the reconstruction results obtained

TABLE 2. Averages and standard deviations of errors calculated by the BP network and ridge regression as a function of the relative uncertainty of the BIX spectra

Relative uncertainty (%)	BP network		Ridge regression	
	Average errors (%)	Standard deviation (%)	Average errors (%)	Standard deviation (%)
0	8.0	8.2	26.5	14.5
1	10.6	8.2	28.3	15.2
3	12.2	8.0	33.3	17.5
5	14.8	8.2	39.2	20.9
8	19.6	9.0	49.3	29.6
10	23.2	10.0	56.0	37.7

by the BP network and ridge regression. Fig. 8(a) shows the initially calculated BIX spectrum of a tritiated titanium sample with a single-energy implantation distribution of tritium compared to the BIX spectrum incorporating 5% and 10% Gaussian noise. The BIX spectra are presented in semi-logarithmic coordinates, and it is apparent that the addition of the relative uncertainty did not change the shape of the BIX spectra. The major effect resulting from the relative uncertainty was an alteration in the intensity ratio between the characteristic peak and bremsstrahlung. Given that the intensity of the characteristic peak was significantly higher than that of the bremsstrahlung, the relative uncertainty resulted in a more pronounced absolute intensity fluctuation in the characteristic peak. As mentioned in Fig. 1 and Fig. 2, the characteristic peak of argon indicates the relative tritium content in the superficial layer beneath the sample surface, and the fluctuation of this peak caused by additional Gaussian noise is likely to result in a larger reconstruction error.

Fig. 8(b–d) show the true and calculated tritium depth profiles using the BP network and ridge regression, which were reconstructed from the original BIX spectrum, BIX spectrum with 5% Gaussian noise, and BIX spectrum with 10% Gaus-
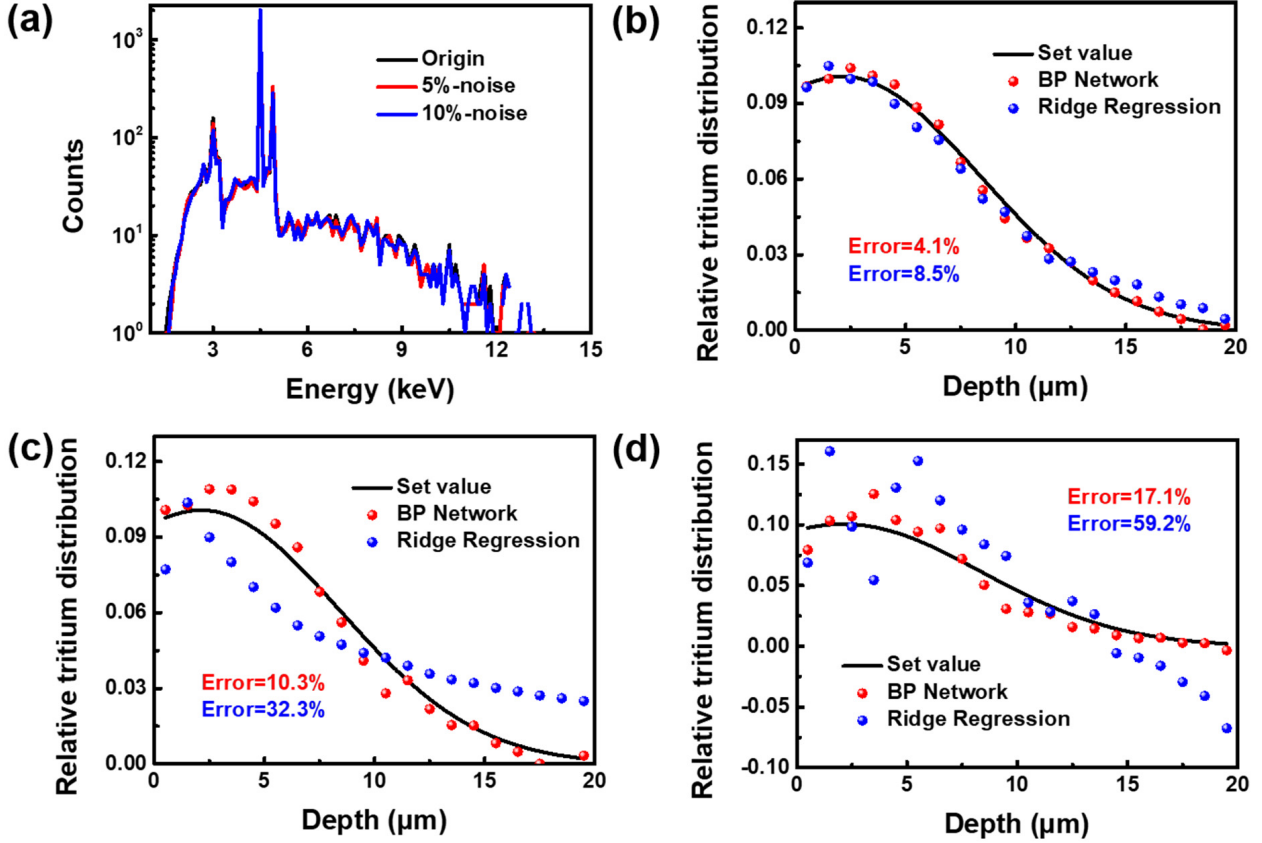
Fig. 8. (Color online) (a) Original calculated BIX spectrum of a titanium sample with a single-energy implantation tritium distribution in semi-logarithmic coordinates (black), compared to the BIX spectrum with 5% (red) and 10% (blue) Gaussian noise. True depth profile of tritium (black curve) compared to the calculated values obtained by the backpropagation network (red scatter plots) and ridge regression (blue scatter plots), reconstructed from the (b) original BIX spectrum, (c) BIX spectrum with 5% Gaussian noise, and (d) BIX spectrum with 10% Gaussian noise.

sian noise, respectively. The reconstruction errors from the original BIX spectrum using the BP network and ridge regression were 4.1% and 8.5%, respectively, as shown in Fig. 8(b). The reconstructed tritium depth profile calculated using the BP network fits well with the true profile. The type of tritium distribution function could be clearly identified, and the peak position of the tritium depth distribution was consistent with the set values. In contrast, the reconstruction error of the tritium depth profile calculated using ridge regression was slightly larger. The relative tritium distribution contents in the superficial layer of the samples calculated using ridge regression were close to the set value, while those in the deeper region had a slightly larger deviation. In this example, the difference in the reconstruction errors calculated using the two methods was not significant when there was no additional Gaussian noise.

When the BIX spectrum had 5% Gaussian noise, the reconstruction error of the tritium depth profile calculated using both the BP network and ridge regression increased, as shown in Fig. 8(c). The reconstruction error calculated using the BP network increased to 10.3%, which remains within an accept-

able range. In addition, the type of tritium distribution function could still be identified from the reconstructed profile. Meanwhile, the reconstruction error calculated using ridge regression increased significantly to 32.3% and the tritium distribution function cannot be discerned between single-energy implantation and unsteady-state diffusion. The disparity in the reconstruction error became more pronounced as the relative uncertainty of BIX spectrum increased to 10%, as shown in Fig. 8(d). The BP network demonstrated robust resistance to noise, as evidenced by a reconstruction error of 17.1%. The reconstructed tritium depth profile remained reliable, and the tritium distribution function could be identified. In contrast, the reconstruction error calculated using ridge regression increased to 59.2%. The calculated tritium depth profile exhibited a high degree of chaos, including negative values. The example shown in Fig. 8 clearly demonstrates the feasibility of training a BP network with robust noise resistance using a BIXS dataset with preset relative uncertainties. This also highlights the advantage of the BP network in accurately and stably reconstructing BIX spectra with a specific level of relative uncertainty.

The findings of this study were based on simulated BIXS data. A crucial factor in validating the accuracy of the BP network method in practical measurements is to guarantee the accuracy of the simulated BIX spectra. We intended to measure the BIX spectra using standard tritiated samples and calibrate the simulated data. Finally, the calibration coefficients were used to generate the BIXS database with high accuracy. Different networks were required for various types of base materials and layer spacings. Selecting an appropriate number of hidden layers within the convergence region guarantees high reconstruction accuracy. The upper limits of the BP network method in the application of BIXS lie in its noise resistance, as additional uncertainty in practical BIXS measurements is inevitable. The uncertainty caused by the uneven distribution on the plane and the X-rays emitted from the activation products in the sample should be considered in future studies.

IV. CONCLUSION

In conclusion, this study demonstrated a highly accurate and reliable reconstruction method for BIXS using a BP network algorithm. A Monte Carlo model was built to simulate the BIX spectra and four different tritium distribution functions with random coefficients were incorporated to generate a training database for the BP network. The number of neurons in the hidden layer of the BP network was optimized to minimize reconstruction errors. The BP network method demonstrated a higher accuracy, broader applicability, and greater noise resistance than the traditional ridge regression method. The average reconstruction error calculated by the BP network was 8.0%, which was much lower than that calculated by ridge regression (26.5%). The BP network method accurately reconstructed BIX spectra of samples with an unknown range of tritium and outperformed the ridge regression across all distribution types. Moreover, the BP network retained higher accuracy and stability than ridge regression with increasing relative uncertainty of the BIX spectra. Our study explored a novel approach for BIXS reconstruction and demonstrated the potential of BIXS for detecting tritium depth profiles in solid materials.

[1] H.X. Wang, X.W. Fu, W.P. Liu et al., Numerical simulation of tritium behavior under a postulated accident condition for CFETR TEP system. Nucl. Sci. Tech. **34**, 109 (2023). doi: 10.1007/s41365-023-01260-w

[2] S.E. Lee, Y. Hatano, M. Hara et al., Tritium distribution analysis of Be limiter tiles from JET-ITER like wall campaigns using imaging plate technique and β-ray induced X-ray spectrometry. Fusion Eng. Des. **160**, 111959 (2020). doi: 10.1016/j.fusengdes.2020.111959

[3] Y.G. Mo, Z.L. Chen, H.H. Song et al., Preliminary analysis of tritium fuel cycle in Z-pinch-driven fusion–fission hybrid reactor. Nucl. Sci. Tech. **29**, 101 (2018). doi: 10.1007/s41365-018-0441-x

[4] M. Röllig, T. Aso, M. Hara et al., Galet – Benchmark of a Geant4 based application for the simulation and design of Beta Induced X-ray Spectrometry systems. Fusion Eng. Des. **143**, 91–98 (2019). doi: 10.1016/j.fusengdes.2019.03.086

[5] A.N. Perevezentsev, A.C. Bell, L.A. Rivkis et al., Comparative study of the tritium distribution in metals. J. Nucl. Mater. **372**, 263–276 (2008). doi: 10.1016/j.jnucmat.2007.03.215

[6] Y.W. Sun, L. Cheng, H.S. Zhou et al., Modelling of deuterium diffusion and thermal desorption in tungsten exposed to high-flux deuterium plasma. Nucl. Sci. Tech. **10**, 106522 (2023). doi: 10.1088/2053-1591/ad02e3

[7] M. Matsuyama, H. Zushi, K. Tokunaga et al., Effect of heating temperature on tritium retention in stainless steel type 316·L. Nucl. Mater. Energy **16**, 52–59 (2018). doi: 10.1016/j.nme.2018.05.024

[8] C.B. Liu, H.S. Zhou, X.C. Li et al., Mixed hydrogen isotopes plasma-driven permeation through CLF-1 RAFM steel for ITER HCCB TBM. Nucl. Fusion **62**, 126017 (2022). doi: 10.1088/1741-4326/ac9193

[9] M. Röllig, B. Bornschein, S. Ebenhöch et al., Geant4 Monte Carlo simulations for sensitivity investigations of an experi-mental facility for the measurement of tritium surface contaminations by BIXS. Fusion Eng. Des. **109**, 684–687 (2016). doi: 10.1016/j.fusengdes.2016.02.018

[10] M. Matsuyama, K. Watanabe,K. Hasegawa. Tritium assay in materials by the bremsstrahlung counting method. Fusion Eng. Des. **39**, 929–936 (1998). doi: 10.1016/S0920-3796(98)00232-4

[11] Y. Yang, Z. Chen, R. Wang et al., Effects of tritium 2-D distribution on tritium depth profile reconstruction in BIXS measurements. Fusion Eng. Des. **130**, 142–147 (2018). doi: 10.1016/j.fusengdes.2018.03.034

[12] Z.L. Chen, P. Huang, Y. Yang et al., Theoretical investigation of tritium concentration quantification method for DT fuel system using β-ray induced X-rays. Fusion Eng. Des. **184**, 113303 (2022). doi: 10.1016/j.fusengdes.2022.113303

[13] M. Matsuyama, T. Tanabe, N. Noda et al., Nondestructive measurements of surface tritium by β-ray induced X-ray spectrometry (BIXS). J. Nucl. Mater. **290**, 437–442 (2001). doi: 10.1016/S0022-3115(00)00581-X

[14] B. Liu, W. Ding, Z. An et al., Tritium analysis in zirconium film with BIXS and EBS: Generality test of Al thin film as the β-ray stopping layer in BIXS. Fusion Eng. Des. **172**, 112751 (2021). doi: 10.1016/j.fusengdes.2021.112751

[15] M. Matsuyama, Y. Torikai, N. Bekris et al., Applicability of β-ray-induced X-ray spectrometry to in situ measurements of tritium retention in plasma-facing materials in ITER. Fusion Eng. Des. **81**, 163–168 (2006). doi: 10.1016/j.fusengdes.2005.08.037

[16] Y. Yang, S.H. Cheng, Y. Li et al., Effects of activation products on tritium measurements for tungsten in fusion reactors. Fusion Eng. Des. **148**, 111276 (2019). doi: 10.1016/j.fusengdes.2019.111276

[17] Z. An, Q. Hou, J. Long. Reconstruction of depth distribution of tritium in materials by β-ray induced X-ray spectrom-

etry. Nucl. Instrum. Meth. B **266**, 3643–3646 (2008). doi: 10.1016/j.nimb.2008.06.020

[18] M. Matsuyama, N. Bekris, M. Glugla et al., Non-destructive tritium measurements of Ml IIA divertors tile by BIXS. J. Nucl. Mater. **313**, 491–495 (2003). doi: 10.1016/S0022-3115(02)01380-6

[19] J. Long, Z. An, Comparison of reconstruction methods of depth distribution of tritium in materials based on BIXS. Nucl. Instrum. Meth. B **267**, 1852–1855 (2009). doi: 10.1016/j.nimb.2009.02.066

[20] Y.S. Hao, Z. Wu, Y.H. Pu et al., Research on inversion method for complex source-term distributions based on deep neural networks. Nucl. Sci. Tech. **34**, 195 (2023). doi: 10.1007/s41365-023-01327-8

[21] H.L. Zheng, X.G. Tuo, S.M. Peng et al., Determination of Gamma point source efficiency based on a back-propagation neural network. Nucl. Sci. Tech. **29**, 195 (2018). doi: 10.1007/s41365-018-0410-4

[22] Y.Y. Cao, J.Y. Guo, B. Zhou, Predictions of nuclear charge radii based on the convolutional neural network. Nucl. Sci. Tech. **34**, 152 (2023). doi: 10.1007/s41365-023-01308-x

[23] L.Y. Zhou, H. Zha, J.R. Shi, A non-invasive diagnostic method of cavity detuning based on a convolutional neural network. Nucl. Sci. Tech. **33**, 94 (2022). doi: 10.1007/s41365-022-01069-z

[24] M. Bouhadida, A. Mazzi, M. Brovchenko et al., Neutron spectrum unfolding using two architectures of convolutional neural networks. Nucl. Eng. Technol. **55**, 2276–2282 (2023). doi: 10.1016/j.net.2023.03.025

[25] A.A. Alvar, M.R. Deevband, M. Ashtiyani. Neutron spectrum unfolding using radial basis function neural networks. Appl. Radiat. Isotopes **129**, 35–41 (2017). doi: 10.1016/j.apradiso.2017.07.048

[26] J. Wang, Y. Zhou, Z. Guo et al., Neutron spectrum unfolding using three artificial intelligence optimization methods. Appl. Radiat. Isotopes **147**, 136–143 (2019). doi: 10.1016/j.apradiso.2019.03.009

[27] G.H. Li, S.Y. Chen, S.L. Jia et al., Prediction of explosives by a de-broadening model based on RBF neural network. Nucl. Instrum. Meth. A **1057**, 168780 (2023). doi: 10.1016/j.nima.2023.168780

[28] Y. Liu, J.J. Zhu, N. Roberts et al., Recovery of saturated signal waveform acquired from high-energy particles with artificial neural networks. Nucl. Sci. Tech. **30**, 148 (2019). doi: 10.1007/s41365-019-0677-0

[29] R.Q. Song, J.F. Han, X.Y. Yan et al., Fast neutron response of 6Li enriched CLYC and CLLB scintillators within 0.9–5.2 MeV. Nucl. Instrum. Meth. A **1055**, 168533 (2023). doi: 10.1016/j.nima.2023.168533

[30] J.P. He, X.B. Tang, P. Gong et al., Spectrometry analysis based on approximation coefficients and deep belief networks. Nucl. Sci. Tech. **29**, 69 (2018). doi: 10.1007/s41365-018-0402-4

[31] W.B. He, Q.F. Li, Y.G. Ma et al., Machine learning in nuclear physics at low and intermediate energies. Sci. China Phys. Mech. **66**, 282001 (2023). doi: 10.1007/s11433-023-2116-0

[32] W.H. Li, P. Ding, W.Q. Xia et al., Artificial neural network reconstructs core power distribution. Nucl. Eng. Technol. **54**, 617 (2022). doi: 10.1016/j.net.2021.08.015

[33] C. Pei, G. Quan, S. Jing et al., An artificial neural network based neutron field reconstruction method for reactor. Ann. Nucl. Energy **138**, 107195 (2020). doi: 10.1016/j.anucene.2019.107195

[34] S. Bagherzadeh-Atashchi, N. Ghal-Eh, F. Rahmani et al., Neutron spectroscopy with TENIS using an artificial neural network. Appl. Radiat. Isotopes **201**, 111035 (2023). doi: 10.1016/j.apradiso.2023.111035

[35] J. Torres-Diaz, G.B. Grad, E.V. Bonzi. Measurement of linear accelerator spectra, reconstructed from percentage depth dose curves by neural networks. Phys. Medica **96**, 81–89 (2022). doi: 10.1016/j.ejmp.2022.02.019

[36] M. Hara, T. Shimura, K. Aoki et al., Monte Carlo simulation of the beta-ray induced X-ray spectra of tritium at various depths in solids. Fusion Eng. Des. **172**, 112814 (2021). doi: 10.1016/j.fusengdes.2021.112814

[37] H. Chen, W. Ding, Z. An et al., BIXS for tritium analysis with Ar gas and Al thin film as β-ray stopping layers and comparison with EBS. Radiat. Phys. Chem. **174**, 108931 (2020). doi: 10.1016/j.radphyschem.2020.108931

[38] M. Brambilla. Quasi-linear ion distribution function during ion cyclotron heating in tokamaks. Nucl. Fusion **34**, 1121–1143 (1994). doi: 10.1088/0029-5515/34/8/I06

[39] I. Youle, A. A. Haasz. Profiling with tritium imaging. J. Nucl. Mater. **248**, 64–71 (1997). doi: 10.1016/S0022-3115(97)00150-5

[40] A.R. Dulloo, W.S. Diethorn. Recoil tritium in 304-stainless steel the initial distribution revisited. J. Nucl. Mater. **256**, 235–246 (1998). doi: 10.1016/S0022-3115(98)00048-8

[41] J.F. Song, Z.Y. Huang, L.X. Li et al., One-dimensional simulation of hydrogen isotopes diffusion in composite materials by FVM. Int. J. Hydrogen Energ. **36**, 5702–5706 (2011). doi: 10.1016/j.ijhydene.2011.02.040